# Magnetic-Field-Driven Surface Electromagnetic States in the Graphene–Antiferromagnetic Photonic Crystal System

**Yu. O. Averkov\*, S. I. Tarapov, V. M. Yakovenko, and V. A. Yampol'skii**

*Usikov Institute of Radiophysics and Electronics, National Academy of Sciences of Ukraine,*
*ul. Akademika Proskury 12, Kharkiv, 61085 Ukraine*
*\*e-mail: yuriyaverkov@gmail.com*
Received June 30, 2014

**Abstract**—The surface electromagnetic states (SEMSs) on graphene, which has a linear carrier dispersion law and is placed in an antiferromagnetic photonic crystal, are theoretically studied in the terahertz frequency range. The unit cell of such a crystal consists of layers of a nonmagnetic insulator and a uniaxial antiferromagnet, the easy axis of which is parallel to the crystal layers. A dc magnetic field is parallel to the easy axis of the antiferromagnet. An expression that relates the SEMS frequencies to the structure parameters is obtained. The problem of SEMS excitation by an external TE-polarized electromagnetic wave is solved, and the dependences of the transmission coefficient on the dc magnetic field and the carrier concentration are constructed. These dependences are shown to differ substantially from the case of a conventional two-dimensional electron gas with a quadratic electron dispersion law. Thus, the positions of the transmission coefficient peaks related to resonance SEMS excitation can be used to determine the character of carrier dispersion law in a two-dimensional electron gas.

**DOI:** 10.1134/S1063776115020016

## 1. INTRODUCTION

Graphene is known to be a two-dimensional allotropic form of carbon, the crystal lattice of which is similar to the structure of honeycomb [1]. The unit cell of this lattice is represented by a regular hexagon with carbon atoms at its vertices. Graphene can be considered as the main structural unit of other allotropic forms of carbon, namely, fullerenes (zero-dimensional objects) [2], quantum nanotubes (one-dimensional objects) [3], and three-dimensional graphite forms (which are represented by graphene stacks bounded by weak van der Waals forces). The structure of the energy bands of graphene and its semimetal conducting properties were theoretically described in 1947 [4]. However, the first graphene films were prepared only 60 years later via multiple mechanical splitting of highly oriented pyrolitic graphite [5]. The uniqueness of work [5] also consists in the fact that it proved the possibility of existence of regular thermodynamically stable 2D crystals, which had been denied for a long time (see, e.g., [6] and Refs. therein).

The main difference of the electronic properties of graphene from those of a conventional 2D electron gas (2DEG; e.g., a thin metallic or semiconductor film) is that graphene is a semimetal with a zero band overlap. The valence band and the conduction band of graphene touch each other at two points in the Brillouin zone (so-called Dirac points). Near these points, the dependence of the carrier energy on the carrier momentum is linear, and charge carriers are massless

chiral Dirac fermions [7–9]. The fermion velocity in graphene is lower than the velocity of light in vacuum by a factor of 300. The Dirac character of charge carriers in graphene, e.g., makes it possible to observe a number of unique effects, such as the anomalous quantum Hall effect (at room temperature) [8], the Klein paradox [10–12], the Aharonov–Bohm effect [13], the Anderson localization [14], and the Coulomb blockage [15]. In strong magnetic fields, exciton gaps [16] and Wigner crystals [17] can form in graphene. Binary graphene layers can exhibit both ferromagnetic and antiferromagnetic properties [18].

These unusual physical properties of graphene are caused by the internal quantum-mechanical features of graphene and, hence, manifest themselves at the quantum level. The quantum-mechanical peculiarities of the transport properties of graphene are also reflected on its "classical" electrodynamic characteristics. For example, Rana [19] proposed a conceptual model for coherent terahertz radiation source, which is based on the inversion electron population of levels in the valence band of graphene due to the interband transitions caused by the interaction of electrons in the valence band with surface plasmons of graphene. The authors of [20] revealed a giant Purcell effect for an elementary dipole located on the surface of a metamaterial consisting of alternating graphene and dielectric layers. It was noted that this effect can be used to significantly increase the terahertz radiation source intensity. The high electron mobility in graphene (up to $10^6$ cm$^2$/(V s) [21]) makes it possible to create

graphene-based active plasmon interferometers and photodetectors that can operate in the frequency range from terahertz to visible radiation and have an extremely high operation speed, a low control voltage, low power consumption, and very small sizes [22].

Mikhailov and Ziegler [23] predicted the ability of graphene to maintain the propagation of TE-polarized surface electromagnetic waves. The physical cause of this ability is a linear law of dispersion of conduction electrons near a Dirac point, and a necessary condition of this ability is a negative imaginary part of the resulting conductivity of graphene.

The purpose of this work is to theoretically study the properties of surface electromagnetic states (SEMSs) localized near graphene and their difference from the properties of SEMSs near 2DEG with a quadratic law of electron dispersion. Recall that SEMSs are electromagnetic oscillations that are uniform along the surface and have a zero tangential wavenumber. The field amplitudes of such oscillations decrease exponentially with the distance from an interface. The possibility of existence of such states was first noted in [24, 25]. The authors of those works were also the first to draw an analogy between SEMSs and the Tamm electron states [26] and to perform experiments on SEMS excitation. Practical interest in SEMSs is related to the possibility to use such the states and structures in which they are present to create resonance optical filters [27], polariton lasers [28], and optical logic devices [29]. Many theoretical and experimental works dealt with the properties of SEMS at the interfaces of a plasmalike medium (PM) and a photonic crystal (PC) [27, 30, 32–37] and at the interface of two PCs [30–32, 38].

The SEMS at the interface between artificial PM and PC in the gigahertz frequency range was experimentally studied for the first time in [34]. The effect of a dc magnetic field on the properties of SEMS at the interface between PM and dielectric PC was theoretically studied in [36]. The properties of SEMS at the interface of magnetic and dielectric PCs and in the PM–ferrite–dielectric PC in a dc magnetic field were comprehensively investigated in [37, 38]. The dispersion properties of SEMS in the structure consisting of a finite number of periodic alternating graphene and dielectric layers were analyzed in [39]. In particular, it was found that these properties depend substantially on the thicknesses of the boundary dielectric layers of the structure.

In [40], we theoretically studied the dispersion characteristics of the TM and TE electromagnetic waves localized near graphene embedded into dielectric PC. It was shown that these waves can coexist in the same frequency range, in contrast to the case where graphene is in a homogeneous dielectric environment (e.g., in vacuum [23]). It was found that a localized TE mode appears in the first bandgap of PC beginning from the IR spectral region, where the imaginary part of the resulting conductivity of graphene becomes negative, despite the asymmetric dielectric environment of graphene. The depths of localization of the electromagnetic fields of TM and TE modes near graphene were compared in the centimeter, terahertz, and IR regions, and the excitation of the corresponding modes by an external electromagnetic wave in a finite PC–graphene–PC structure was investigated.

In contrast to [40], in this work we theoretically study the spectral properties of SEMS on graphene placed in antiferromagnetic PC in an external dc magnetic field. Prominence was given to an analysis of the magnetic field dependences of the transmission spectrum of an antiferromagnetic PC–2DEG–antiferromagnetic PC structure, which differ qualitatively for 2DEGs with linear and quadratic dispersion laws. In particular, we showed that the behavior of the dependences of the position of the transmission coefficient peaks that correspond to SEMS excitation in the bandgap of PC on the carrier concentration in 2DEG is qualitatively close to the behavior of the corresponding dependences for the Fermi energy. A fundamentally new result of this work is thought to be the fact that the properties of SEMS in antiferromagnetic PCs and the effects of resonance excitation of these states by an external electromagnetic wave can be effectively driven by an external dc magnetic field. For example, we showed that, when studying the magnetic-field dependence of the transmission spectrum of antiferromagnetic PC with embedded 2DEG, one can determine the type of carrier dispersion law in 2DEG, i.e., a linear (for graphene) or quadratic (e.g., for a thin graphite film, metal, or semiconductor) law.

For SEMS to be excited on graphene, the oscillation frequencies should not be much lower than pulsed electron relaxation frequency $\nu$, which is rather high due to the effect of a substrate (e.g., $\nu \sim 10^{13}$ s$^{-1}$ for conventional "non-suspended" graphene [41, 42]). Terahertz or higher frequencies meet this condition. Therefore, the most convenient material for the formation of a magnetic PC is an antiferromagnet, the resonance frequencies in which can lie in the submillimeter region of the electromagnetic spectrum [43]. We consider the case of low temperatures well below Néwel temperature $T_N$. Numerical calculations were performed for antiferromagnetic iron difluoride FeF$_2$ with $T_N \approx 78$ K at liquid-helium temperatures [44].

## 2. FORMULATION OF THE PROBLEM AND BASIC EQUATIONS

The coordinate system is chosen so that axis $y$ is directed along the normal to antiferromagnetic PC layers and external dc magnetic field $\mathbf{H}_0$ is directed along axis $z$ (Fig. 1). The unit cell of antiferromagnetic PC consists of an antiferromagnet and a nonmagnetic insulator with layer thicknesses $d_1$ and $d_2$, respectively. The period of the antiferromagnetic PC structure is $d = d_1 + d_2$. Graphene is located in plane $y = Nd$, i.e.,

at the boundary between the $(N-1)$th and $N$th cells of antiferromagnetic PC. For clarity, Fig. 1 schematically shows graphene as a layer of a finite width. The antiferromagnet is nonconducting and is described by permittivity $\varepsilon_1$ and magnetic permeability tensor $\boldsymbol{\mu}$. The nonmagnetic insulator is described by permittivity $\varepsilon_2$. The easy axis of the antiferromagnet is parallel to axis $z$, i.e., vector $\mathbf{H}_0$. We consider the Voigt geometry, where an electromagnetic wave propagates in plane $xy$ perpendicular to the easy axis of the ferromagnet and, correspondingly, to the dc magnetic field direction. Let a TE-polarized wave have field components $\mathbf{E} = (0, 0, E_z)$ and $\mathbf{H} = (H_x, H_y, 0)$. The dc magnetic field is assumed to be lower than critical field $H_{sf}$ at which a spin-flop transition proceeds in the antiferromagnet [45]. We also neglect the dissipative losses in the antiferromagnetic PC layers.

Maxwell equations for the fields in the antiferromagnet region are written as

$$\operatorname{curl}\mathbf{E} = -\frac{1}{c}\frac{\partial \mathbf{B}}{\partial t}, \quad \operatorname{div}\mathbf{B} = 0, \tag{1}$$

$$\operatorname{curl}\mathbf{H} = \frac{\varepsilon_1}{c}\frac{\partial \mathbf{E}}{\partial t}, \quad \operatorname{div}\mathbf{E} = 0, \tag{2}$$

where vectors $\mathbf{B}$ and $\mathbf{H}$ are related to each other by a certain constitutive equation. When specifying electromagnetic wave fields in the form

$$\mathbf{E}_\ell = \mathbf{E}_{0\ell}\exp[i(k_x x + k_{\ell y}y - \omega t)], \quad \ell = 1, 2, \tag{3}$$

we can write this constitutive equation as $B_j = \mu_{jk}H_k$, where tensor $\boldsymbol{\mu}$ is [44, 45]

$$\boldsymbol{\mu} = \begin{pmatrix} \mu & i\mu_a & 0 \\ -i\mu_a & \mu & 0 \\ 0 & 0 & 1 \end{pmatrix}, \tag{4}$$

$$\mu = 1 + \frac{\omega_m\omega_a}{\omega_1^2 - \omega_+^2} + \frac{\omega_m\omega_a}{\omega_1^2 - \omega_-^2}, \tag{5}$$

$$\mu_a = \frac{\omega_m\omega_a}{\omega_1^2 - \omega_+^2} - \frac{\omega_m\omega_a}{\omega_1^2 - \omega_-^2}, \tag{6}$$

where $\omega_m = 4\pi\gamma M_0$, $\omega_a = \gamma H_a$, $\omega_\pm = \omega \pm \gamma H_0$;

$$\omega_1 = \gamma\sqrt{H_a(2H_{ex} + H_a)}, \tag{7}$$

where $\gamma$ is the gyromagnetic ratio, $M_0$ is the sublattice magnetization, and $H_a$ and $H_{ex}$ are the effective anisotropy and exchange fields, respectively. Note that critical field $H_{sf}$ at which a spin-flop transition proceeds in the antiferromagnet is written as

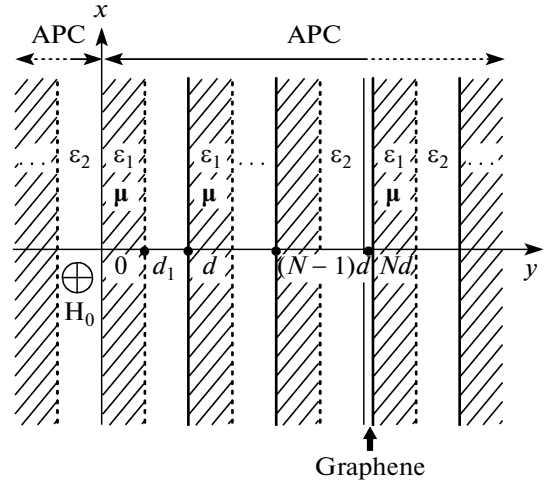$$H_{sf} = \sqrt{2H_a H_{ex}}. \tag{8}$$



**Fig. 1.** Geometry of the problem (APC is the antiferromagnetic photonic crystal).

From Maxwell equations (1) and (2), we obtain the following expressions for electric field component $E_z$ and magnetic field components $H_x$ and $H_y$:

$$E_z = A_1\exp(ik_{1y}y) + A_2\exp(-ik_{1y}y), \tag{9}$$

$$H_x = \frac{c}{\omega}[a_1 A_1\exp(ik_{1y}y) - a_2 A_2\exp(-ik_{1y}y)], \tag{10}$$

$$H_y = -\frac{c}{\omega}[b_1 A_1\exp(ik_{1y}y) - b_2 A_2\exp(-ik_{1y}y)], \tag{11}$$

where

$$a_1 = \frac{\mu k_{1y} + i\mu_a k_x}{\mu^2 - \mu_a^2}, \quad a_2 = \frac{\mu k_{1y} - i\mu_a k_x}{\mu^2 - \mu_a^2}, \tag{12}$$

$$b_1 = \frac{\mu k_x - i\mu_a k_{1y}}{\mu^2 - \mu_a^2}, \quad b_2 = -\frac{\mu k_x + i\mu_a k_{1y}}{\mu^2 - \mu_a^2}, \tag{13}$$

$$k_{1y} = \sqrt{\frac{\omega^2}{c^2}\varepsilon_1\mu_{eff} - k_x^2}, \quad \mu_{eff} = \frac{\mu^2 - \mu_a^2}{\mu}. \tag{14}$$

Factor $\exp[i(k_x x - \omega t)]$ will be omitted in Eqs. (9)–(11) and the subsequent field equations.

In the region of the nonmagnetic insulator ($\mu_2 = 1$), the Maxwell equations are described by Eqs. (1) and (2), where vector $\mathbf{H}$ substitutes for vector $\mathbf{B}$, permittivity $\varepsilon_2$ substitutes for $\varepsilon_1$, and field equations have the form

$$E_z = C_1\exp(ik_{2y}y) + C_2\exp(-ik_{2y}y), \tag{15}$$

$$H_x = \frac{ck_{2y}}{\omega}[C_1\exp(ik_{2y}y) - C_2\exp(-ik_{2y}y)], \tag{16}$$

$$H_y = -\frac{ck_x}{\omega}[C_1\exp(ik_{2y}y) + C_2\exp(-ik_{2y}y)], \tag{17}$$

$$k_{2y} = \sqrt{\frac{\omega^2}{c^2}\varepsilon_2 - k_x^2}. \tag{18}$$

Using the approach developed in [46] to describe the coupled Tamm states on a crystal surface, we represent the fields in the region $y > Nd$ as the superposition of incident and reflected waves,

$$E_{\Sigma, z}^{(\text{R})}(y) = A_{\text{in}} E_{z, \text{in}}^{(\text{R})}(y) \exp[-ik(y - Nd)]$$
$$+ A_{\text{r}} E_{z, r}^{(\text{R})}(y) \exp[ik(y - Nd)], \qquad (19)$$

$$H_{\Sigma, x}^{(\text{R})}(y) = A_{\text{in}} H_{x, \text{in}}^{(\text{R})}(y) \exp[-ik(y - Nd)]$$
$$+ A_{\text{r}} H_{x, r}^{(\text{R})}(y) \exp[ik(y - Nd)], \qquad (20)$$

where $k$ is the Bloch wavenumber [47], the first terms in Eqs. (19) and (20) correspond to the fields of the wave incident on the interface $y = Nd$, and the second terms correspond to the fields of the wave reflected from the interface $y = Nd$. Superscript "R" means that fields belong to the region on the right of the plane $y = Nd$ of graphene. Constant $A_{\text{in}}$ is taken to be specified and constant $A_{\text{r}}$ is to be determined from boundary conditions. The fields of the transmitted wave (in the region $y < Nd$, i.e., the region with superscript "L") are written in the form

$$E_z^{(\text{L})}(y) = A_{\text{tr}} E_{z, \text{tr}}^{(\text{L})}(y) \exp[-ik(y - Nd)], \qquad (21)$$

$$H_x^{(\text{L})}(y) = A_{\text{tr}} H_{x, \text{tr}}^{(\text{L})}(y) \exp[-ik(y - Nd)], \qquad (22)$$

where constant $A_{\text{tr}}$ is to be determined from boundary conditions. Expressions for fields $E_{z, \text{in}}^{(\text{R})}(y)$, $E_{z, r}^{(\text{R})}(y)$; $H_{x, \text{in}}^{(\text{R})}(y)$, $H_{x, r}^{(\text{R})}(y)$; and $E_{z, \text{tr}}^{(\text{L})}(y)$, $H_{x, \text{tr}}^{(\text{L})}(y)$ are given in [37].

The fields in antiferromagnetic PC satisfy the Bloch relation

$$\begin{pmatrix} E_z[(N+1)d] \\ H_x[(N+1)d] \end{pmatrix} = \exp(\pm ikd) \begin{pmatrix} E_z(Nd) \\ H_x(Nd) \end{pmatrix} \qquad (23)$$

and the translation condition [47]

$$\begin{pmatrix} E_z[(N+1)d] \\ H_x[(N+1)d] \end{pmatrix} = \mathbf{M}^{(TE)} \begin{pmatrix} E_z(Nd) \\ H_x(Nd) \end{pmatrix}, \qquad (24)$$

where $\mathbf{M}^{(\text{TE})}$ is the TE wave propagation matrix and $\cos(kd) = (M_{11}^{(\text{TE})} + M_{22}^{(\text{TE})})/2$ [47]. Let $\text{Im} k > 0$. In this case, the sign "plus" in the exponent in Eq. (23) corresponds to the wave propagating in the positive direction of axis $y$, and the sign "minus" corresponds to the wave propagating in the negative direction of axis $y$.

With conditions (23) and (24), we can find the relation between the components of the electric and magnetic fields at the interface $y = Nd$ in the following two equivalent forms:

$$E_z(Nd) = \frac{\exp(\pm ikd) - M_{22}^{(\text{TE})}}{M_{21}^{(\text{TE})}} H_x(Nd), \qquad (25)$$

$$E_z(Nd) = \frac{M_{12}^{(\text{TE})}}{\exp(\pm ikd) - M_{11}^{(\text{TE})}} H_x(Nd). \qquad (26)$$

From the conditions of continuity of the tangential components of the electric and magnetic fields at the boundaries of the PC layers, we find the following expressions for the matrix $\mathbf{M}^{(\text{TE})}$ components:

$$M_{11}^{(\text{TE})} = \left[ \cos(k_{1y}d_1) + \frac{\mu_a k_x}{\mu k_{1y}} \sin(k_{1y}d_1) \right] \cos(k_{2y}d_2)$$
$$- \frac{(\mu k_{1y})^2 + (\mu_a k_x)^2}{\mu k_{1y}k_{2y}(\mu^2 - \mu_a^2)} \sin(k_{1y}d_1) \sin(k_{2y}d_2), \qquad (27)$$

$$M_{12}^{(\text{TE})} = \frac{i\omega}{c} \frac{\mu^2 - \mu_a^2}{\mu k_{1y}} \sin(k_{1y}d_1) \cos(k_{2y}d_2)$$
$$+ \frac{i\omega}{ck_{2y}} \left[ \cos(k_{1y}d_1) - \frac{\mu_a k_x}{\mu k_{1y}} \sin(k_{1y}d_1) \right] \sin(k_{2y}d_2), \qquad (28)$$

$$M_{21}^{(\text{TE})} = \frac{ick_{2y}}{\omega} \left[ \cos(k_{1y}d_1) + \frac{\mu_a k_x}{\mu k_{1y}} \sin(k_{1y}d_1) \right] \sin(k_{2y}d_2)$$
$$+ \frac{ic}{\omega} \frac{(\mu k_{1y})^2 + (\mu_a k_x)^2}{\mu k_{1y}(\mu^2 - \mu_a^2)} \sin(k_{1y}d_1) \cos(k_{2y}d_2), \qquad (29)$$

$$M_{22}^{(\text{TE})} = -\frac{k_{2y}(\mu^2 - \mu_a^2)}{\mu k_{1y}} \sin(k_{1y}d_1) \sin(k_{2y}d_2)$$
$$+ \left[ \cos(k_{1y}d_1) - \frac{\mu_a k_x}{\mu k_{1y}} \sin(k_{1y}d_1) \right] \cos(k_{2y}d_2). \qquad (30)$$

We write boundary conditions in the graphene plane in the form

$$E_{\Sigma, z}^{(\text{R})}(Nd) = E_z^{(\text{L})}(Nd), \qquad (31)$$

$$H_{\Sigma, x}^{(\text{R})}(Nd) - H_x^{(\text{L})}(Nd) = -\frac{4\pi}{c} \sigma E_z^{(\text{L})}(Nd), \qquad (32)$$

where $\sigma$ is the electrical conductivity of graphene, which is the sum of the intraband ($\sigma^{\text{intra}}$) and interband ($\sigma^{\text{inter}}$) conductivities [48]. For a degenerate electron gas ($k_B T \ll E_F$, where $k_B$ is the Boltzmann constant, $T$ is the temperature, and $E_F$ is the Fermi energy), conductivities $\sigma^{\text{intra}}$ and $\sigma^{\text{inter}}$ are determined from the expressions [48]

$$\sigma^{\text{intra}} = \frac{ie^2 E_F}{\pi \hbar^2 (\omega + i\nu)}, \qquad (33)$$

$$\sigma^{\text{inter}}$$
$$= \frac{e^2}{4\hbar} \left[ \theta(\hbar\omega - 2E_F) - \frac{i}{2\pi} \ln \frac{(\hbar\omega + 2E_F)^2}{(\hbar\omega - 2E_F)^2 + (2k_B T)^2} \right], \qquad (34)$$

$$E_F = \hbar\nu\sqrt{\pi n}, \qquad (35)$$

where $\nu = 10^8$ cm/s, $n$ is the carrier concentration in graphene, and $\theta(x)$ is the Heaviside function [49].

During passage through the graphene plane, the propagation matrix has the form

$$\mathbf{M}^{(Gr)} = \begin{pmatrix} 1 & 0 \\ -\dfrac{4\pi\sigma}{c} & 1 \end{pmatrix}. \qquad (36)$$

We find the Fresnel transmission coefficient in the region $y < Nd$. The vanishing of the denominator of this coefficient corresponds to the excitation of a surface electromagnetic wave (at $k_x \neq 0$). Therefore, setting the denominator of the Fresnel transmission coefficient of an electromagnetic wave equal to zero, we derive a dispersion equation for surface electromagnetic waves. At $k_x = 0$, this equation describes the properties of SEMS in the structure under study.

When meeting boundary conditions (31) and (32), we obtain the following expression for Fresnel transmission coefficient $t_F$ of surface electromagnetic waves in the region $y < Nd$:

$$t_F = \frac{\sin(kd)}{\sin(kd) - \dfrac{2\pi i\sigma}{c}M_{12}^{(TE)}}. \qquad (37)$$

Therefore, the dispersion equation for such waves takes the form

$$\sin(kd) = \frac{2\pi i\sigma}{c}M_{12}^{(TE)}. \qquad (38)$$

From here on, we will analyze the properties of SEMS in the presence of a dc magnetic field by numerical solution of Eq. (38) at $k_x = 0$.

We now analyze the structure consisting of $2N$ unit cells and graphene located at the center of the structure that is located in a nonmagnetic dielectric with permittivity $\varepsilon_d$. Energy transmission coefficient $D_{2N}$ for an electromagnetic wave that is incident on this structure from the side of positive values of $y$ is expressed as

$$D_{2N} = \frac{2}{F_{11} + F_{22} - \dfrac{ck_{dy}}{\omega}F_{12} - \dfrac{\omega}{ck_{dy}}F_{21}}, \qquad (39)$$

where $k_{dy} = \sqrt{\varepsilon_d\omega^2/c^2 - k_x^2}$ and

$$\mathbf{F} = (\mathbf{M}^{(TE)})^N \mathbf{M}^{(Gr)} (\mathbf{M}^{(TE)})^N. \qquad (40)$$

## 3. NUMERICAL ANALYSIS OF THE SEMS EQUATION

We now numerically analyze Eq. (38) at $k_x = 0$ and $\nu = 0$ and construct the dependences of the SEMS frequencies on the external magnetic field. To this end, we introduce dimensionless frequency $\Omega = \omega/\omega_0$, where $\omega_0 \approx 0.995\omega_1$, and chose the following material parameters of the media composing antiferromagnetic PC. As the antiferromagnetic medium, we chose iron difluoride $FeF_2$ [44]: $\varepsilon_1 \approx 5.5$, $\omega_1 \approx 1.6 \times 10^{12}$ s$^{-1}$, $\gamma = 3.15 \times 10^6$ s$^{-1}$ Oe$^{-1}$, $H_a \approx 200$ kOe, $H_{ex} \approx 540$ kOe, $H_{sf} \approx$



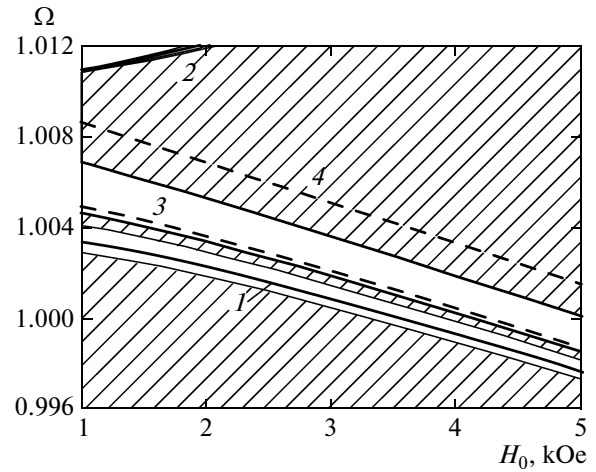**Fig. 2.** Dimensionless SEMS frequency vs. dc magnetic field.

465 kOe, and $M_0 = 560$ G. As the nonmagnetic insulator, we chose quartz glass with $\varepsilon_2 \approx 3.8$ [50]. The structure temperature is taken to be $T = 4.2$ K, which is well below the Néel temperature.

Figure 2 shows the $\Omega(H_0)$ dependences (curves *1*, *2*) for $d_1 = d_2 = 0.45c/\omega_0$ and the electron concentration $n = 10^{12}$ cm$^{-2}$ ($E_F \approx 1350$ K) in graphene. The shaded regions in Fig. 2 correspond to the allowed bands of antiferromagnetic PC, and the white regions correspond to the bandgaps of antiferromagnetic PC. Curve *1* is located in the first bandgap and curve *2*, in the third bandgap. Curve *3* corresponds to the condition $|\mu_{eff}| \longrightarrow \infty$ and curve *4*, to the condition $\mu_{eff} = 0$. In the region between curves *3* and *4*, we have $\mu_{eff} < 0$ and $\text{Re}(k_{1y}) = 0$. As is seen from Fig. 2, the character of the $\Omega(H_0)$ changes qualitatively when the bandgap number increases. Using antiferromagnetic PC as the medium surrounding the graphene plane, we can detect SEMS excitation at a fixed frequency when an external electromagnetic wave is incident on the structure along the normal by changing the dc magnetic field.

## 4. NUMERICAL ANALYSIS OF THE FIELD DEPENDENCE OF THE TRANSMISSION COEFFICIENT

We now analyze the dependences of energy transmission coefficient $D_{2N}$ on external magnetic field $H_0$ at $k_x = 0$ and $\varepsilon_d = 1$ for various carrier concentrations $n$ in graphene.

Figure 3 shows the $D_{2N}(H_0)$ dependences for antiferromagnetic PC with $N = 10$, $d_1 = d_2 = 0.45c/\omega_0$, $\Omega = 1$, and $\nu = 10^{13}$ s$^{-1}$ for various values of $n$. SEMS excitation corresponds to peaks *A* and *B*. It is seen that, as the carrier concentration increases, the SEMS peak shifts into the bandgap, its magnitude decreases, and the peak becomes more diffuse. The last circum-
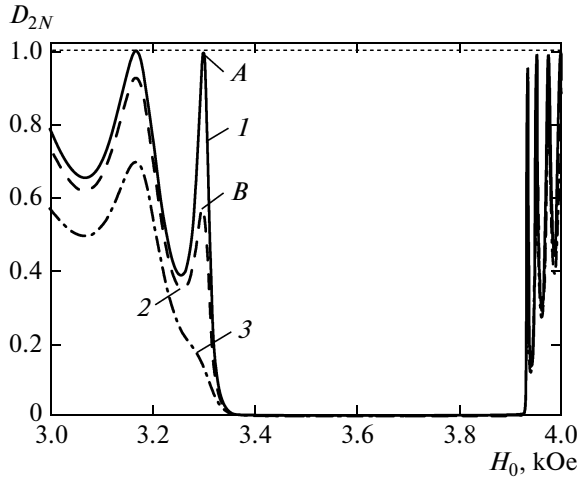
**Fig. 3.** Dependence $D_{2N}(H_0)$ for $n = (1)$ $10^9$, $(2)$ $10^{11}$, and $(3)$ $5 \times 10^{11}$ cm$^{-2}$.
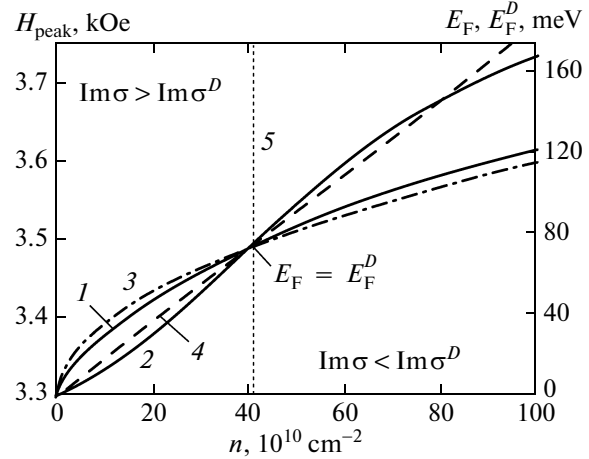


**Fig. 4.** Positions of the peaks corresponding to SEMS excitation and the Fermi energy vs. $n$ for 2DEG with a linear or quadratic electron dispersion law.

stance is related to a sufficiently high relaxation frequency $\nu$. Note that concentration $n$ can be changed by the application of gate voltage to graphene [5].

Assume that 2DEG, the carrier dispersion law in which can be both linear (graphene) and quadratic (e.g., semiconductor), is located at the center of the structure under study. In the former case, the conductivity of the conducting layer is described by Eqs. (33) and (34); in the latter case, it is described by the Drude formula for a degenerate electron gas,

$$\sigma^D = \frac{ie^2 E_F^D}{\pi \hbar^2 (\omega + i\nu)}, \quad E_F^D = \frac{\pi \hbar^2 n}{m}, \quad (41)$$

where $n$, $m$, and $E_F^D$ are the concentration, the effective mass, and the Fermi energy of electrons in 2DEG, respectively. For an electron gas with a quadratic carrier dispersion law, the equation that describes the properties of SEMS and the expression for the transmission coefficient are determined from Eqs. (38) and (39), where $\sigma$ should be replaced by $\sigma^D$.

Let us analyze the dependence of dc magnetic fields $H_{\text{peak}}$ corresponding to the SEMS peaks on the carrier concentration for 2DEG with a linear or a quadratic carrier dispersion law. Figure 4 shows the $H_{\text{peak}}(n)$, $E_F(n)$, and $E_F^D(n)$ dependences for antiferromagnetic PC with $N = 10$, $d_1 = d_2 = 0.45c/\omega_0$, $\Omega = 1$, $\nu/\omega_0 \ll \Omega$, and $m = 0.013m_0$ (InSb semiconductor, $m_0$ is the free electron mass). In Fig. 4, curve $1$ corresponds to the $H_{\text{peak}}(n)$ dependence for 2DEG with a linear electron dispersion law, curve $2$, to the $H_{\text{peak}}(n)$ dependence for 2DEG with a quadratic electron dispersion law; curve $3$, to the $E_F(n)$ dependence; and curve $4$, to the $E_F^D(n)$ dependence. Line $5$ corresponds to an electron concentration $n_{\text{tr}} \approx 4.1 \times 10^{11}$ cm$^{-2}$ in

2DEG, and the equality $E_F = E_F^D$ holds true at this concentration. As is seen in Fig. 4, the $H_{\text{peak}}(n)$ dependence for 2DEG with a linear electron dispersion law is qualitatively close to the dependence $E_F(n) \propto \sqrt{n}$, and the $H_{\text{peak}}(n)$ dependence for 2DEG with a quadratic dispersion law is close to the dependence $E_F^D(n) \propto n$. This finding means that the behavior of the $H_{\text{peak}}(n)$ dependence points to a qualitative character of an electron dispersion law in 2DEG. Note that the inequality $\text{Im}\sigma > \text{Im}\sigma^D$ is satisfied in the range $n < n_{\text{tr}}$ and the inequality $\text{Im}\sigma < \text{Im}\sigma^D$ is satisfied in the range $n > n_{\text{tr}}$. Note also that the condition $\text{Im}\sigma > 0$ is met for the chosen graphene parameters and a frequency $\Omega = 1$. When the real losses in graphene (when the $\nu/\omega_0$ ratio is higher than or on the order of frequency $\Omega$) are taken into account, the behavior of the dependences considered above is retained but the values of $n$ at which SEMS peaks are detected is bounded by the range $10^9$ cm$^{-2} \le n < 5 \times 10^{11}$ cm$^{-2}$.

Figure 5 shows the distributions of the squared moduli of the complex amplitudes of the electric and magnetic fields in SEMS and the distribution of the energy transmission coefficient along the structure with graphene at $k_x = 0$, $N = 10$, $d_1 = d_2 = 0.45c/\omega_0$, $\Omega = 1$, $\nu = 10^{13}$ s$^{-1}$, $n = 10^{12}$ cm$^{-2}$, and $\varepsilon_d = 1$. A wave is incident on the structure from the side of cell 20 and graphene is placed in the plane $y = 10d$. As is seen in Fig. 5, the envelopes of $|E_z|^2$ and $|H_x|^2$ (Fig. 5b, curve $1$) begin to decrease during the motion deep into the structure beginning from cell 20 and do not increase when the graphene plane is approached, as in the case of the SEMS field distribution near the PM−PC (or two different PCs) interface (see, e.g., [30, 32]). This circumstance is related to a high value of frequency $\nu$. High dissipative losses of the electromagnetic field in
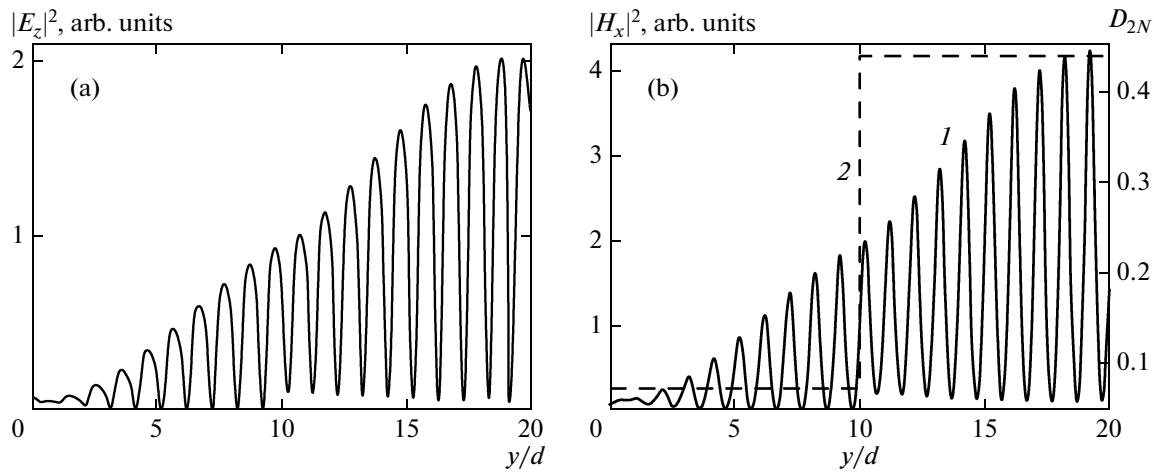
$|E_z|^2$, arb. units

(a)

$|H_x|^2$, arb. units

$D_{2N}$

(b)

*2*

*1*

$y/d$

$y/d$

**Fig. 5.** Distributions (a) $|E_z(y)|^2$ and (b) (*1*) $|H_x(y)|^2$ and (*2*) $D_{2N}$ along the structure for $N = 10$.

the graphene plane lead to an approximately sixfold jumplike decrease of $D_{2N}$ at $y = 10d$ (Fig. 5b, curve *2*).

## 5. CONCLUSIONS

The spectrum of SEMSs was theoretically studied in the terahertz frequency range near graphene placed in antiferromagnetic PC in the presence of a dc magnetic field. A relation that connects the SEMS frequencies to the parameters of graphene and the antiferromagnetic PC was obtained, and an expression for the coefficient of transmission of an electromagnetic wave through such a structure with a finite number of elementary cells was derived. The dependences of the positions of transmission coefficient maxima on the magnetic field and the carrier concentration in 2DEG with a linear or a quadratic electron dispersion law were compared. The behavior of these dependences was found to agree qualitatively with the behavior of the dependence of the Fermi energy on the carrier concentration in 2DEG with the corresponding electron dispersion law. This means that, when analyzing the dependences of the position of the transmission coefficient on the magnetic field and the carrier concentration in 2DEG, one can draw a conclusion regarding the character of the carrier dispersion law.

## REFERENCES

1. A. H. Castro Neto, F. Guinea, N. M. R. Peres, K. S. Novoselov, and A. K. Geim, Rev. Mod. Phys. **81**, 109 (2009).

2. W. Andreoni, in *Physics and Chemistry of Materials with Low-Dimensional Structures*, Ed. by F. Levy and E. Mooser (Springer, Berlin, 2000), Vol. 23, p. 448.

3. R. Saito, G. Dresselhaus, and M. S. Dresselhaus, *Physical Properties of Carbon Nanotubes* (Imperial College Press, London, 1998), p. 259.

4. P. R. Wallace, Rev. Mod. Phys. **71**, 622 (1947).

5. K. S. Novoselov, A. K. Geim, S. V. Morozov, D. Jiang, Y. Zhang, S. V. Dubonos, I. V. Grigorieva, and A. A. Firsov, Science (Washington) **306**, 666 (2004).

6. J. C. Meyer, A. K. Geim, M. I. Katsnelson, K. S. Novoselov, T. J. Booth, and S. Roth, Nature (London) **446**, 60 (2007).

7. A. K. Geim and K. S. Novoselov, Nat. Mater. **6**, 183 (2007).

8. K. S. Novoselov, A. K. Geim, S. V. Morozov, D. Jiang, M. I. Katsnelson, I. V. Grigorieva, S. V. Dubonos, and A. A. Firsov, Nature (London) **438**, 197 (2005).

9. Y. Zhang, Y. W. Tan, H. L. Stormer, and P. Kim, Nature (London) **438**, 201 (2005).

10. M. I. Katsnelson, K. S. Novoselov, and A. K. Geim, Nat. Phys. **2**, 620 (2006).

11. V. V. Cheianov, V. I. Fal'ko, and B. L. Altshuler, Science (Washington) **315**, 1252 (2007).

12. C. W. J. Beenakker, Rev. Mod. Phys. **80**, 1337 (2008).

13. P. Recher, B. Trauzettel, A. Rycerz, Ya. M. Blanter, C. W. J. Beenakker, and A. F. Morpurgo, Phys. Rev. B: Condens. Matter **76**, 235404 (2007).

14. S. V. Morozov, K. S. Novoselov, M. I. Katsnelson, F. Schedin, L. A. Ponomarenko, D. Jiang, and A. K. Geim, Phys. Rev. Lett. **97**, 016801 (2006).

15. F. Sols, F. Guinea, and A. H. Castro Neto, Phys. Rev. Lett. **99**, 166803 (2007).

16. V. P. Gusynin, V. A. Miransky, S. G. Sharapov, and I. A. Shovkovy, Phys. Rev. B: Condens. Matter **74**, 195429 (2006).

17. C.-H. Zhang and Y. N. Joglekar, Phys. Rev. B: Condens. Matter **75**, 245414 (2007).

18. N. M. R. Peres, F. Guinea, and A. H. Castro Neto, Phys. Rev. B: Condens. Matter **72**, 174406 (2005).

19. F. Rana, IEEE Trans. Nanotechnol. **7**, 91 (2008).

20. I. V. Iorsh, I. S. Mukhin, I. V. Shadrivov, P. A. Belov, and Y. S. Kivshar Phys. Rev. B: Condens. Matter **87**, 075416 (2013).

21. A. S. Mayorov, D. C. Elias, M. Mucha-Kruczynski, R. V. Gorbachev, T. Tudorovskiy, A. Zhukov, S. V. Morozov, M. I. Katsnelson, V. I. Fal'ko, A. K. Geim, and

K. S. Novoselov, Science (Washington) **333**, 860 (2011).

22. A. N. Grigorenko, M. Polini, and K. S. Novoselov, Nat. Photonics **6**, 749 (2012).

23. S. A. Mikhailov and K. Ziegler, Phys. Rev. Lett. **99**, 016803 (2007).

24. A. A. Bulgakov and V. R. Kovtun, Opt. Spectrosc. **56** (5), 471 (1984).

25. A. A. Bulgakov and V. R. Kovtun, Solid State Commun. **56**, 781 (1985).

26. I. E. Tamm, Phys. Z. Sowjetunion **1**, 733 (1932).

27. M. E. Sasin, R. P. Seisyan, and M. A. Kaliteevski, Superlattices Microstruct. **47**, 44 (2010).

28. A. Kavokin, I. Shelykh, and G. Malpuech, Appl. Phys. Lett. **87**, 261105 (2005).

29. I. Iorsh, P. V. Panicheva, V. A. Slovinskii, and M. A. Kaliteevski, Tech. Phys. Lett. **38** (4), 351 (2012).

30. A. P. Vinogradov, A. V. Dorofeenko, S. G. Erokhin, M. Inoue, A. A. Lisyansky, A. M. Merzlikin, and A. B. Granovsky, Phys. Rev. B: Condens. Matter **74**, 045128 (2006).

31. T. Goto, A. V. Dorofeenko, A. M. Merzlikin, A. V. Baryshev, A. P. Vinogradov, M. Inoue, A. A. Lisyansky, and A. B. Granovsky, Phys. Rev. Lett. **101**, 113902 (2008).

32. A. P. Vinogradov, A. V. Dorofeenko, A. M. Merzlikin, and A. A. Lisyansky, Phys.—Usp. **53** (3), 243 (2010).

33. F. G. Bass and A. P. Tetervov, Phys. Rep. **140**, 237 (1986).

34. D. P. Belozorov, M. K. Khodzitsky, and S. I. Tarapov, J. Phys. D: Appl. Phys. **42**, 055003 (2009).

35. Yu. O. Averkov, N. N. Beletskii, and V. M. Yakovenko, Radiofiz. Elektron. (Kharkov) **2** (16), 40 (2011).

36. Yu. O. Averkov, N. N. Beletskii, S. I. Tarapov, et al., Radiofiz. Elektron. (Kharkov) **3** (17), 48 (2012).

37. Yu. O. Averkov, S. I. Tarapov, A. A. Kharchenko, and V. M. Yakovenko, Low Temp. Phys. **40** (7), 667 (2014).

38. S. I. Tarapov and D. P. Belozorov, Low Temp. Phys. **38** (7), 603 (2012).

39. D. Smirnova, P. Buslaev, I. Iorsh, I. V. Shadrivov, P. A. Belov, and Y. S. Kivshar, Phys. Rev. B: Condens. Matter **89**, 245414 (2014).

40. Yu. O. Averkov, V. M. Yakovenko, V. A. Yampol'skii, and Franco Nori, Phys. Rev. B: Condens. Matter **90**, 045415 (2014).

41. Y.-W. Tan, Y. Zhang, K. Bolotin, Y. Zhao, S. Adam, E. H. Hwang, S. Das Sarma, H. L. Stormer, and P. Kim, Phys. Rev. Lett. **99**, 246803 (2007).

42. X. Hong, K. Zou, and J. Zhu, Phys. Rev. B: Condens. Matter **80**, 241415 (2009).

43. A. S. Borovik-Romanov, *Lectures on Low-Temperature Magnetism* (Moscow State University, Moscow, 2010), p. 48 [in Russian].

44. F. Lima, T. Dumelow, E. L. Albuquerque, and J. A. P. da Costa, J. Opt. Soc. Am. B **28**, 306 (2011).

45. E. A. Turov, A. V. Kolchanov, V. V. Men'shenin, I. F. Mirsaev, and V. V. Nikolaev, *Symmetry and Physical Properties of Antiferromagnets* (Fizmatlit, Moscow, 2001), p. 131 [in Russian].

46. I. M. Lifshitz and S. I. Pekar, Usp. Fiz. Nauk **56**, 531 (1955).

47. F. G. Bass, A. A. Bulgakov, and A. P. Tetervov, *High-Frequency Properties of Semiconductors with Superlattices* (Nauka, Moscow, 1989), p. 23 [in Russian].

48. L. A. Falkovsky, J. Exp. Theor. Phys. **106** (3), 575 (2008).

49. M. Abramowitz and I. Stegun, *Handbook of Mathematical Functions: With Formulas, Graphs, and Mathematical Tables* (Dover, New York, 1965; Nauka, Moscow, 1979), p. 807.

50. A. P. Babichev, N. A. Babushkina, A. M. Bratkovskii, et al., in *Handbook of Physical Quantities*, Ed. by I. S. Grigoriev and E. Z. Melikhov (Energoatomizdat, Moscow, 1991; CRC Press, Boca Raton, Florida, United States, 1997), p. 549.

*Translated by K. Shakhlevich*